Chapter 4

The Interstellar Medium in Isolated Galaxies

4.1 Introduction

In this chapter we apply the physical model developed in chapter 3 to the simulation of isolated galaxies. We perform simulations of both isolated quiescent galactic disks and of the collapse of dark matter/baryonic haloes. We find that the sticky particle model is very successful in reproducing many of the observed properties of disk galaxies, including the molecular cloud mass spectrum, the molecular fraction as a function of radius, the Schmidt law, the stellar density profile and the appearance of a galactic fountain. We find that the ISM created by the sticky particle model is tightly self-regulating and stable; and that simulations of an initially quiescent disk remain stable over many years, with an almost contant SFR, which slowly decreases due to having used up the gas in the disk.

In the second part of this chapter we observe the effects on the galaxy of including differing physics in our implementation.

4.2 Quiescent Disk

One of the fundamental properties that a star formation prescription must be able to reproduce is that in MW like conditions, the resulting behaviour should be similar to that in the MW. In this section we discuss the properties of galaxy simulations set up to approximate the conditions in the MW's quiescent disk.

4.2.1 Simulation Details

We set up a simplified model of a MW type galaxy using initial conditions from GalactICS (Kuijken and Dubinski (1995)). GalactICS generates near equilibrium distributions

Resolution ($M_\odot$)	*Disk*	*Bulge*	*Halo*
Low	6.6×10^6	5.84×10^6	5.6×10^6
Base	8.3×10^5	7.5×10^5	7.1×10^5
High	1.0×10^5	9.2×10^4	1.0×10^5

Table 4.1: Initial particle masses in three different realisations of the model GalactICs galaxy that are used throughout this paper. The disk, bulge and halo consist entirely of baryons, the halo additionally contains dark matter. All masses are in units of $M_\odot$. Baryons are added to the dark matter halo by converting a random 1% of the particles into gas, so the dark matter particle mass in the halo is the same as the gas particle mass.

of collisionless particles consisting of a disk, bulge and halo. These models consist of a spherical bulge component; an approximately exponential disk, which is rotationally supported in the x-y plane and supported by random motion in the z direction; and an approximately spherical halo.

We add baryonic material to this distribution by converting the disk and bulge in their entirety into SPH particles at a temperature of $10^4 K$. 1% of the material in the halo is converted to baryons with a temperature of $10^6 K$. The addition of baryonic material puts the system well out of equilibrium so each simulation is run adiabatically for 250Myr to allow the galaxy to relax closer to its equilibrium state before the additional physics is allowed to operate. The total mass in the disk, bulge and halo are $1 \times 10^{10} M_\odot$, $0.43 \times 10^{10} M_\odot$ and $1.1 \times 10^{11} M_\odot$ respectively. The mass resolution of particles in each of three realisations of this galaxy are summarised in table 4.1. These masses were chosen such that the gaseous particles in each of the three components have approximately the same mass and the dark matter halo particles have masses as close as possible to the gas particle mass. The gravitational softenings for the disk particles (that is: gas, sticky and star) is set to 0.1kpc, 0.05kpc and 0.02kpc in simulations GAL_LORES, GAL_BASE and GAL_HIRES respectively. The dark matter particles have softening lengths ten times larger than the disk particles.

The GalactICS simulations provide a test of the code in a situation somewhat similar to a quiescent MW disk. As discussed in section 3.2, all simulations were performed with the entropy conserving SPH code GADGET2 (Springel (2005)), with all of the physics

Name	Details	N_{gas}
GAL_BASE	Base GalactICs model	19330
GAL_LORES	Base model with degraded mass resolution	2450
GAL_HIRES	Base model with improved mass resolution	255000
GAL_BASE_LOSN	E_{51} decreased by factor of 5	19330
GAL_BASE_HISN	E_{51} increased by factor of 5	19330
GAL_BASE_LOCON	Conduction efficiency decreased by factor of 5	19330
GAL_BASE_HICON	Conduction efficiency increased by factor of 5	19330
GAL_BASE_LOZ	Gas metallicity set to 0.5 Solar	19330
GAL_BASE_HIZ	Gas metallicity set to 1.5 Solar	19330
ROT_BASE	Spherical rotating collapse	15000
ROT_LORES	Spherical rotating collapse	4000
ROT_HIRES	Spherical rotating collapse	45000

Table 4.2: Brief table of simulation references and details. N_{gas} shows the number of gas particles in the disk, bulge and halo combined.

discussed in section 3.2 implemented as additional modules. Table 4.2 contains a brief summary of the different simulations. Typical timestep size in one of the base simulations is $\sim 10^4$yr, although this figure is smaller at early times when bursts of supernovae heat gas very strongly.

4.2.2 The Base Simulations

In this section we will discuss simulations run with the base set of physical parameters (section 3.3.1). Most simulations were run at the base mass resolution as defined in table 4.1.

The large scale behaviour of the model galaxy is as follows: Immediately after switching on the additional star formation physics the dense, thermally unstable gas in the disk and bulge collapses into cold clouds, which quickly collapse, causing a large burst of star formation. After approximately 500Myr the galaxy settles down into a quiescent state with a star formation rate of approximately $1M_{\odot}/$yr. The star formation rate gradually decreases as the cold gas in the galaxy is consumed by stars.

It is known that in the MW, most areas of active star formation are concentrated in the
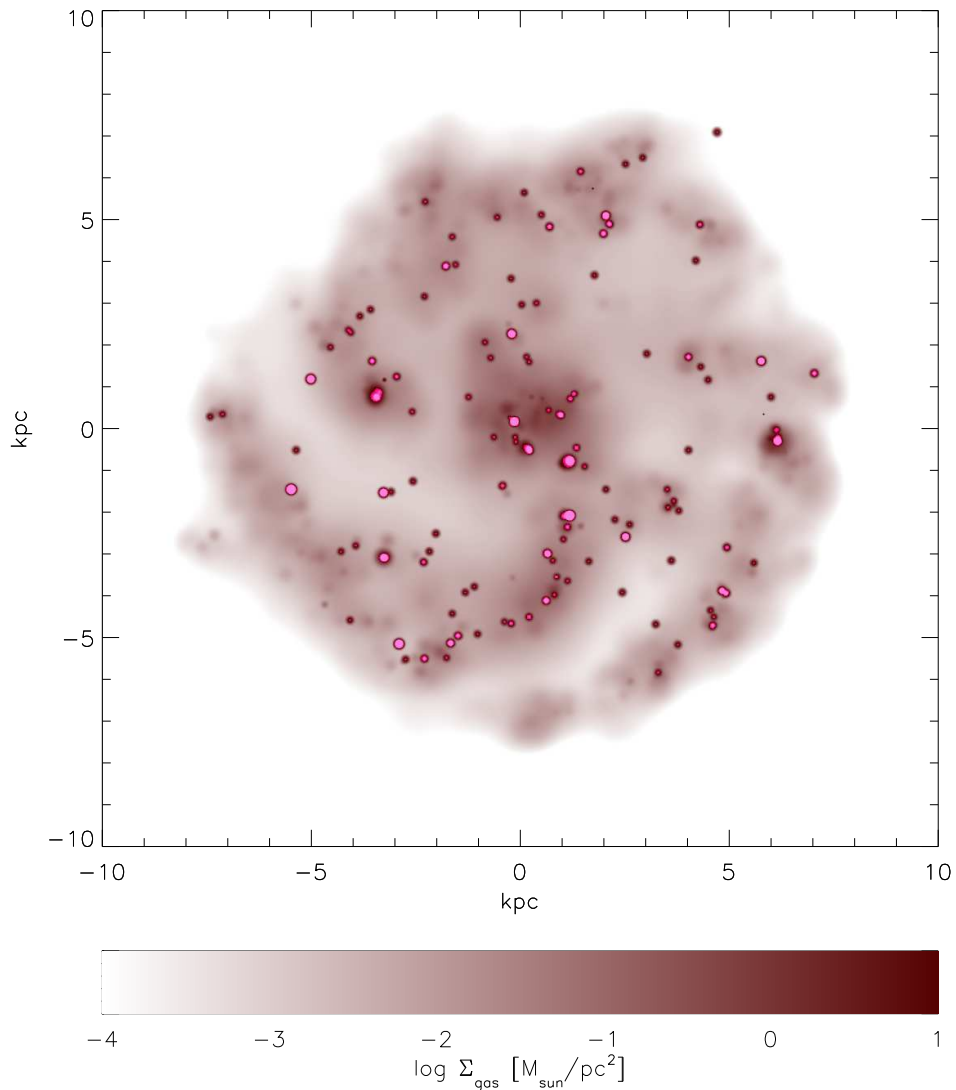
Figure 4.1: Demonstration of the star formation properties of the isolated galactic disk. The continuous field represents the molecular gas surface density of the simulated galactic disk, spiral structure is evident. The circles represent the locations of all stars formed within the last 10Myr. Most star formation events represent the collapse of a single GMC, resulting in the formation of $10^5 M_\odot$ of stars. It is clear that star formation is occurring primarily in the spiral arms of the galaxy.
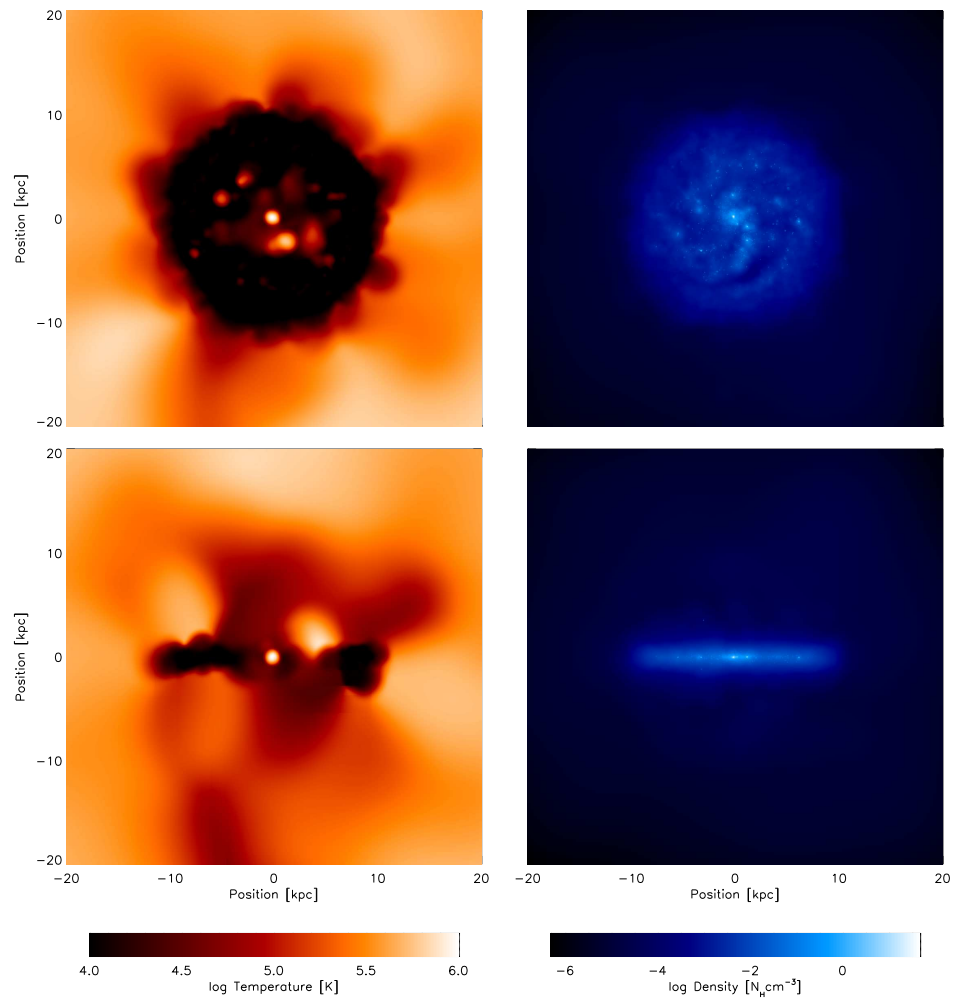
Figure 4.2: A thin slice of the gas temperature and density distributions after 1Gyr in run GAL_BASE. The slice is taken directly through the centre of mass of the stellar disk. The temperature plot clearly shows regions of strongly heated gas, these are areas near to sites of active star formation, where the massive, shortly lived stars are undergoing SNe.
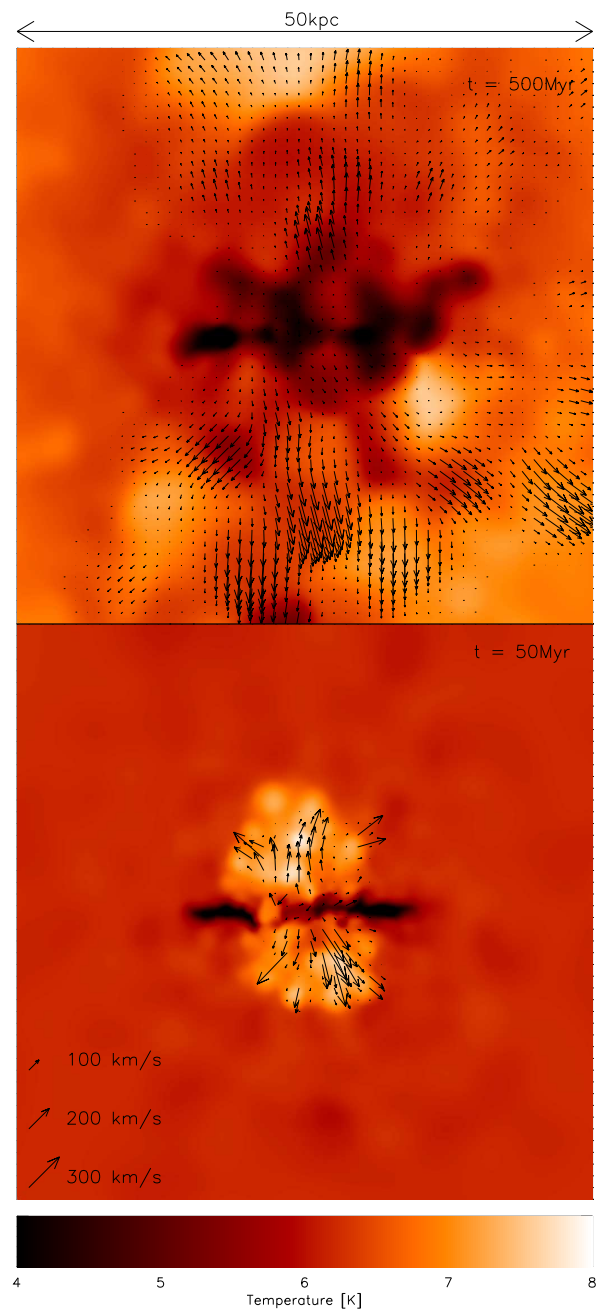
Figure 4.3: A thin slice of the gas temperature field through the centre of a disk galaxy simulation. The arrows represent the gas velocity field, taking into account only gas that has been heated by supernovae. The generation of bipolar outflows from the galactic disk is very clear. The lower plot represents the galaxy after 50Myr, the upper panel is the same galactic disk after 500Myr.
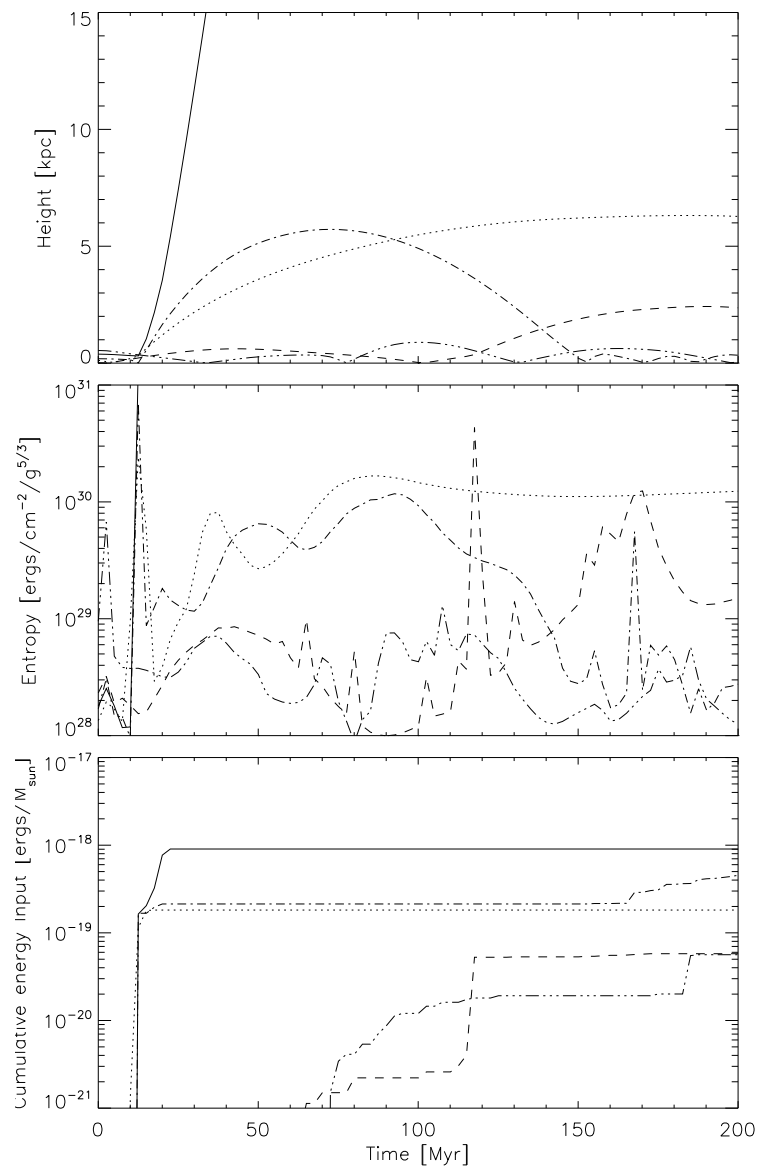
Figure 4.4: Relationship between the number of supernova heatings and the distance from the mid-plane of the disk for a sampling of five particles from the simulated galaxy. Each different linestyle represents a different SPH particle. The top panel shows the perpendicular distance from the centre of the stellar disk, the central panel shows the entropy of each particle and the lower panel the cumulative amount of thermal energy that has been dumped into the particle. It is clear that some particles with a higher entropy are lifted away from the galactic disk where they cool and rain back down on the galactic disk within a hundred Myr of being supernova heated. Other particles are ejected violently from the galaxy, their density becomes very low and they evolve adiabatically.
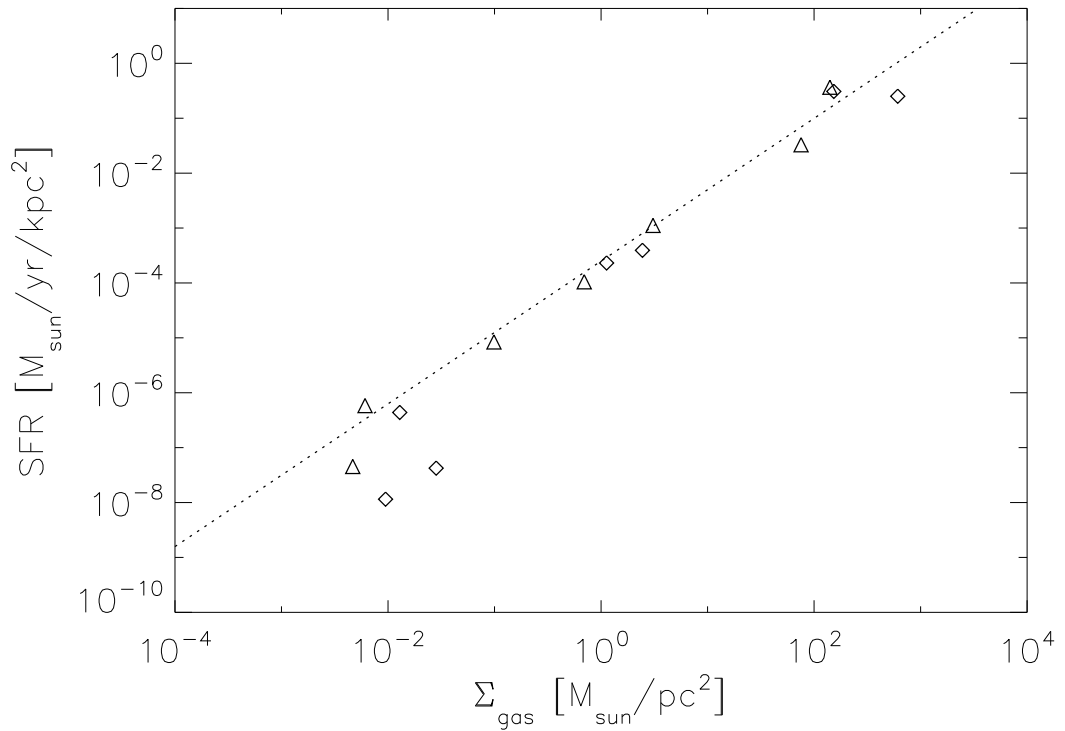
Figure 4.5: The density-star formation rate relationship for our simulated quiescent disk. The diamond shaped points represent the observed star formation rates after 200Myr, and the triangles represent the star formation rates in the same disk after 1Gyr. The dashed line is the observed Schmidt law due to Kennicutt (1998). Our galaxy is in good agreement with the observed Schmidt law throughout its lifetime.
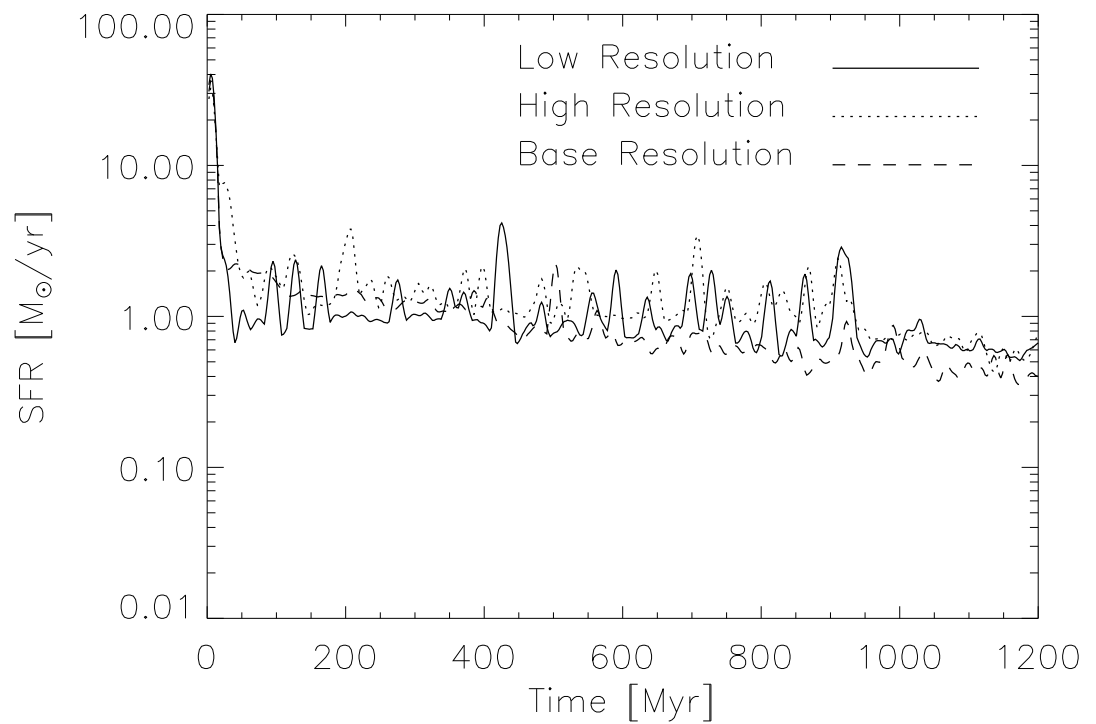
Figure 4.6: Star formation rate as a function of time for isolated galaxy models with different mass resolutions. The mass resolution is 64 times better in the high resolution disk than the low resolution one. The three simulations plotted are GAL_LORES, GAL_BASE and GAL_HIRES. The fact that the star formation rate remains almost unchanged shows that numerical convergence has been achieved.
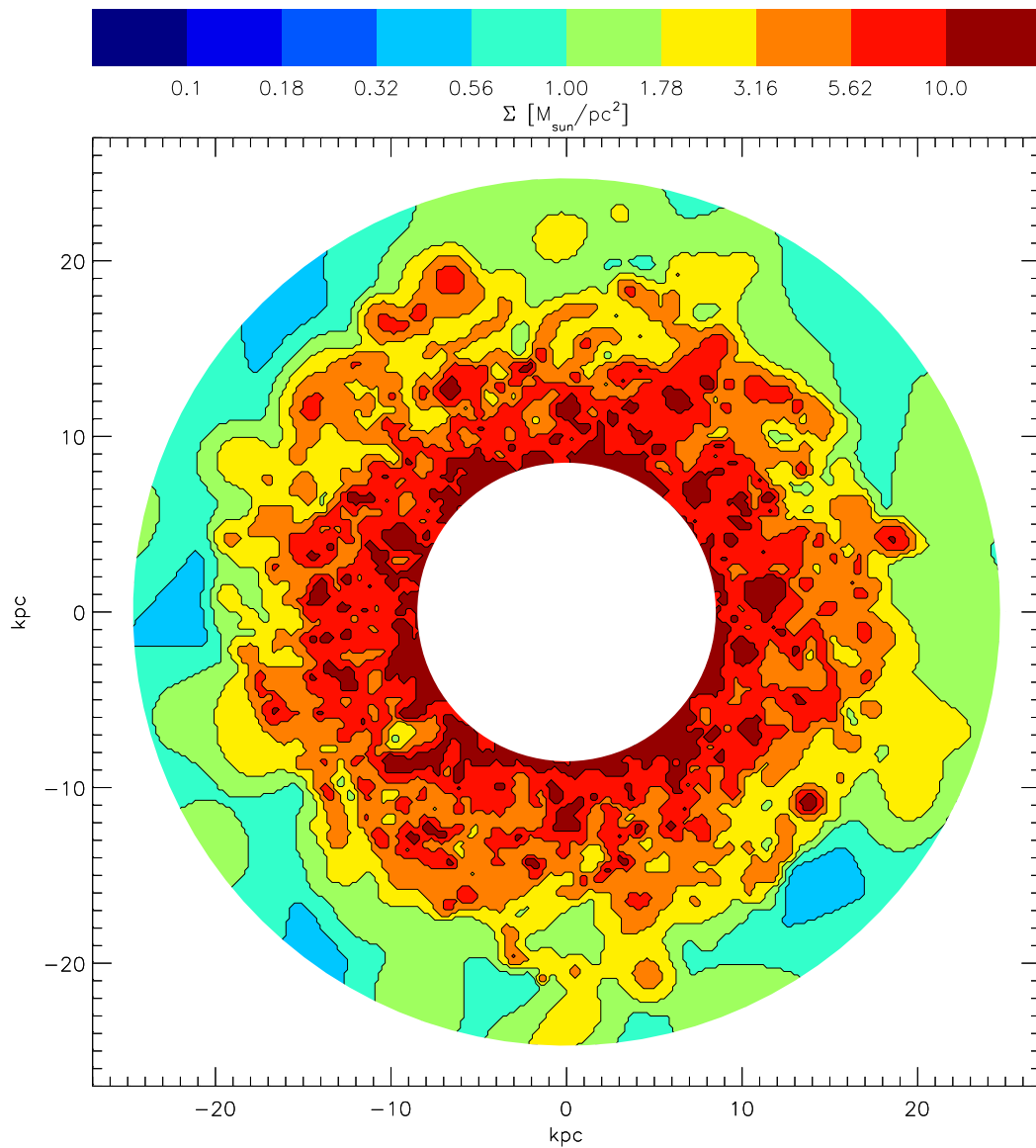
Figure 4.7: Plot of the distribution of atomic gas in a galactic disk. Colours and plot dimensions are matched to those in Levine et al (2006) for easy comparison to observations. The inner circle represents the radius from the centre of the galaxy to the position of the sun. The outer radius is where the observations of Levine et al (2006) are truncated. The simulated MW has a surface density profile in close agreement with that observed by Levine et al.

galactic spiral arms (e.g. Engargiola et al. (2003)). Fig (4.1) shows that our simulations reproduce this behaviour. In the sticky particle model this behaviour occurs naturally as the converging gas flows in galactic spiral arms lead to an increased merger rate and, therefore, to the presence of more star forming clouds. Face and edge on temperature and density plots of the standard resolution galaxy are shown in Fig (4.2). The gas heated by SNII is preferentially situated perpendicular to the plane of the disk, suggesting that the feedback scheme is preferentially heating the low density gas and setting up strong outflows. Fig (4.3) shows the behaviour of the supernova heated gas in a thin slice through the centre of the disk. Initially there is a strong burst of star formation (lower panel of Fig (4.3)), followed shortly by a burst of supernova explosions that heat the gas around the galactic disk as hot at 10^8K. Most of this gas is driven straight out of the halo in a direction perpendicular to the galactic disk. Later on, as the supernova rate dies down, gas is heated more gently and is ejected from the galactic disk in the form of a fountain reminiscent of the galactic fountains present in the MW. This behaviour is demonstrated in figure 4.4, which shows for a random subset of particles from the gas disk the number of times they have been heated as a function of time with their height above the galactic disk. It is clear that upon being strongly heated, some particles are ejected from the galactic disk and fall back down a few hundred Myr later. Others remain in dense regions and cool immediately. Some escape the disk completely in the form of a galactic wind. This behaviour was also observed in the multiphase star formation models of Scannapieco et al. (2006), suggesting that it is a more general feature of multiphase models.

Additionally our simulated galaxies are in good agreement with the observed Schmidt law, Eq (4.5). This behaviour arises due to the self-regulation of the simulated ISM. At higher densities more molecular clouds are formed and so star formation rates are higher. Runaway star formation is prevented by various forms of stellar feedback, which prevent too many clouds from forming. The slope of the Schmidt law in the simulated galaxies may be changed by altering the value of v_{stick}. Higher values of v_{stick} lead to clouds coagulating more rapidly, and so low density regions of the galactic disk undergo more star formation. The effect is less severe in the higher density regions of the galaxy as strong feedback from large bursts of star formation can effectively regulate the amount of star formation. Conversely a lower value of v_{stick} leads to a steeper Schmidt law with a lower overall star formation rate. This behaviour is demonstrated in Fig (3.5) for the one zone model. The value of v_{stick} used to reproduce the Schmidt law slope

and normalisation in the one zone model also works in the simulated galaxy and the observed galaxy follows the observed Schmidt law very closely throughout its whole lifetime (figure (4.5)). In this figure we do not observe a cutoff in star formation rate at a density of $10\mathrm{cm}^{-3}$ as observed in local galaxies. This anomaly is due to the averaging procedure used when calculating star formation rates and densities. Since we do not store star formation rates on a particle-by-particle basis radial bins were used and star formation rates were calculated from the rate of change of stellar mass in each radial bin. This means that although a given radial bin may have a low density on average it may contain some dense star forming knots.

The resolution independence of the star formation prescription is once again demonstrated by Fig (4.6). The star formation rate between the highest and lowest mass resolution simulations is in remarkably good agreement. The general form followed by all simulations is that there is a strong burst of star formation at the initial time, this is rapidly quenched by supernova feedback, and a self-regulating ISM is set up. The star formation rate slowly increases as the gas in the galactic disk is either used up or ejected in the form of winds.

Recent observations of the gas content of the MW have allowed the construction of maps of its gas surface density (Levine et al. (2006)). In order to compare the properties of our model to observations, another GalactICs model was generated with properties as close as possible to those of the MW. The total mass of the galactic disk was set to $5 \times 10^{10} M_\odot$, and the scale radius of the exponential disk to $4.5\mathrm{kpc}$. This simulation was evolved for 1Gyr. The resulting gas distribution is shown in Fig (4.7). Our simulations are in good agreement with the observations of Levine et al. (2006).

These properties suggest that the star formation and feedback prescriptions behave well in a quiescent disk, a more robust test of how they perform in a more general situation is given by the rotating collapse simulations.

4.3 Rotating Collapse

4.3.1 Simulation Details

The second simulation we investigate is the collapse of a rotating spherical halo (Navarro and White (1993)) with an initial $1/r$ density profile consisting of 90% collisionless dark matter and 10% baryonic material. The mass of the rotating sphere is $1 \times 10^{12} M_\odot$ and its initial radius is 100kpc. Velocities are chosen such that the sphere is initially rotating
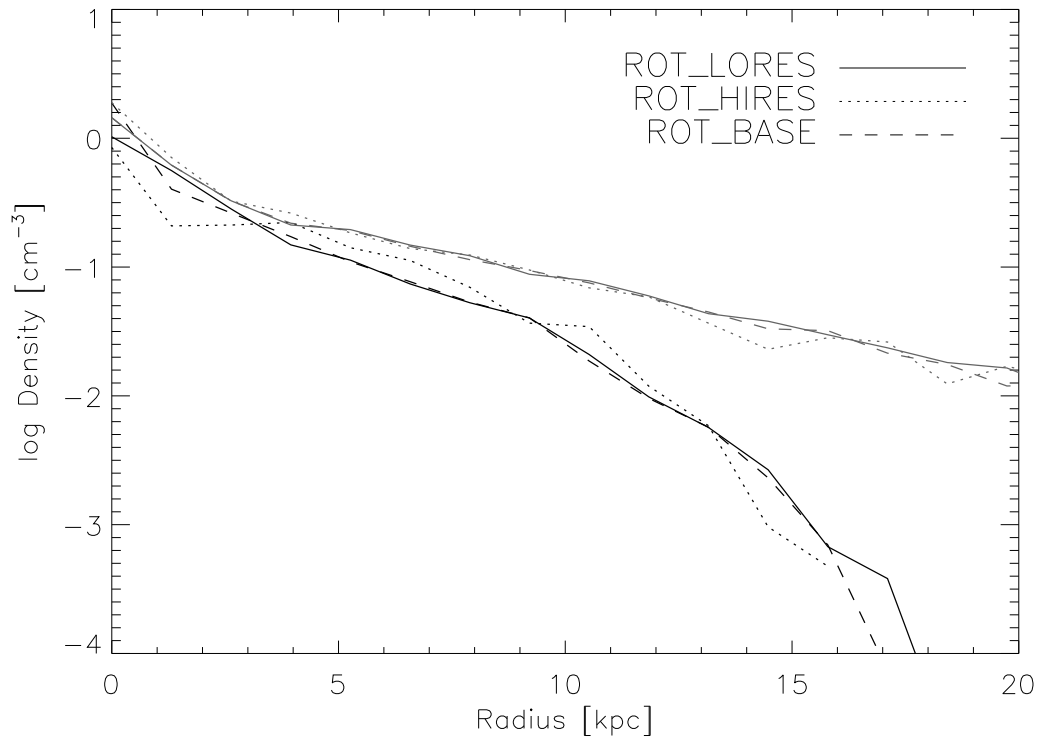
Figure 4.8: Density profiles for the hot, diffuse gas (grey lines) and the cold molecular clouds (black lines). The solid lines represent the low resolution rotating collapse simulations and the dotted lines represent the highest resolution simulations. Agreement between the high and low resolution simulations is very good.

as a solid body with a spin parameter of 0.1. Once again this simulation is created at three different mass resolutions, corresponding to dark matter particle masses of $5.2 \times 10^8 M_\odot$, $5.8 \times 10^7 M_\odot$ and $2.0 \times 10^7 M_\odot$, with corresponding gravitational softenings of 1.93kpc, 0.96kpc and 0.68kpc. The rotating collapse simulations model, in a crude way, the collapse of a protogalaxy, and allow us to investigate how the ISM model behaves when it is initially far from equilibrium and in situations with strong shocks and rapid density changes.

4.3.2   The Base Simulations

After 2Gyr the density profiles of each of the three phases of matter are shown in figure (4.8) and figure (4.9). The density profiles are averaged around the disk; each radial bin represents a ring centered on the centre of mass of the disk. Figure (4.8) shows the radial density profiles of the hot and cold gas. The three different resolution simulations once
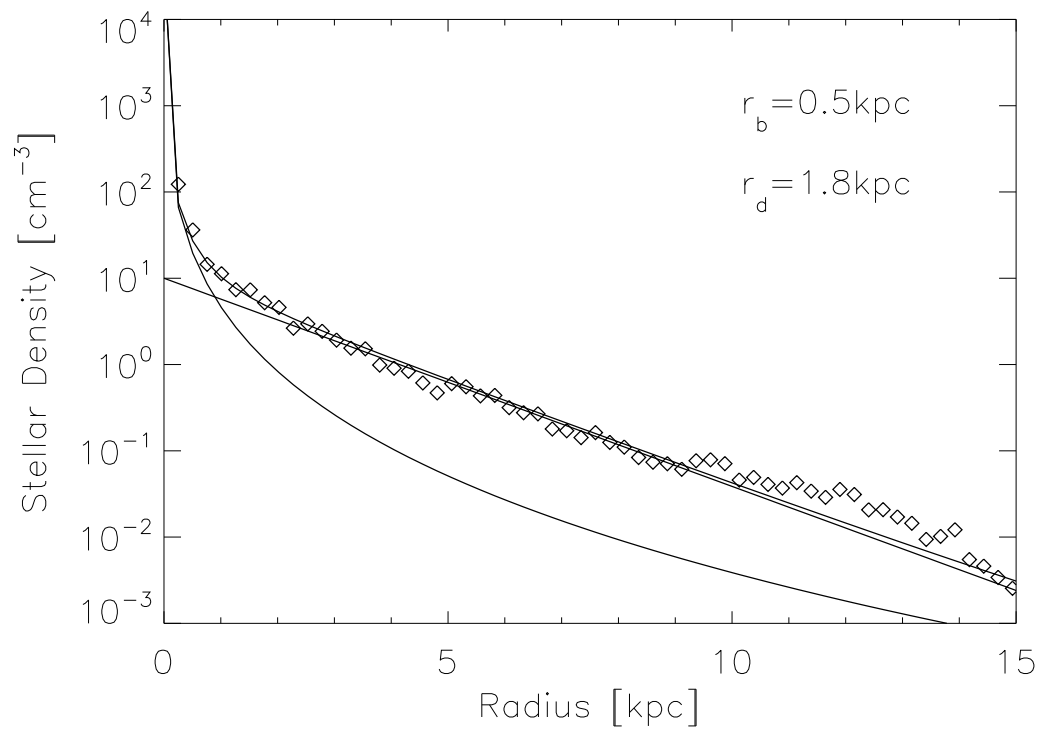
Figure 4.9: Stellar density profile in the base rotating collapse simulation. Solid lines represent the best fit exponential and a de Vacouleurs profile. The scale radii used in the exponential and de Vacouleurs fits are r_d and r_b respectively. It is clear that even starting from an initial condition far from equilibrium we generate a stellar disk with a surface density profile similar to that in observed galaxies.
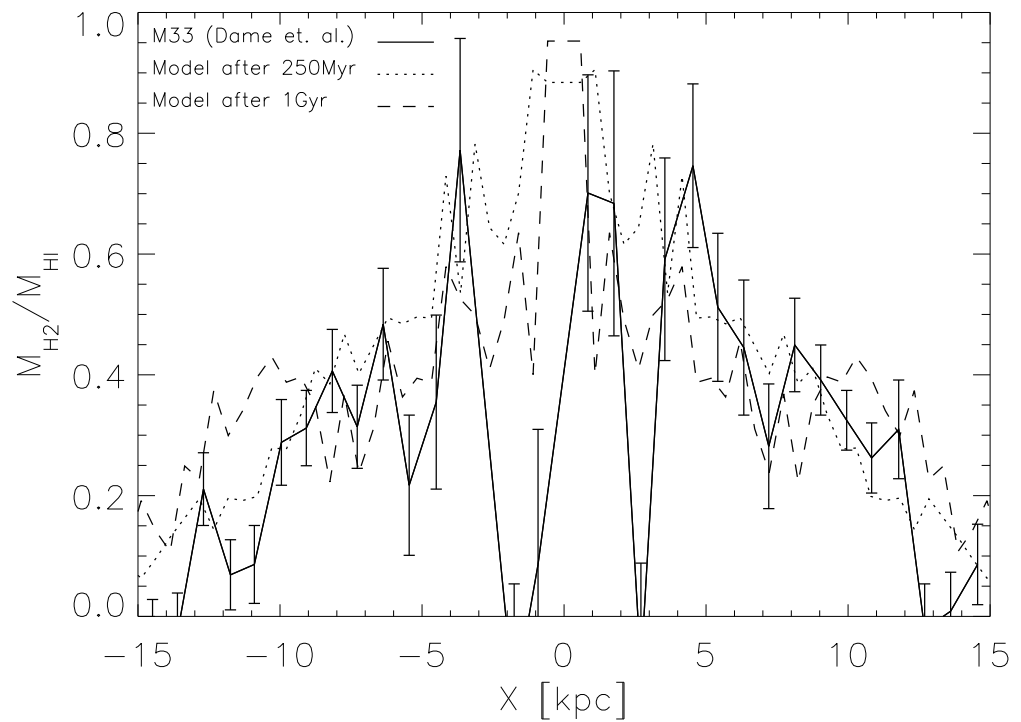
Figure 4.10: Fraction of gas in the molecular phase as a function of distance from the centre of the galactic disk for the rotating collapse model at two different times. The solid line represents the same data as plotted from M33. The simulated galactic disk is in good agreement with observation.
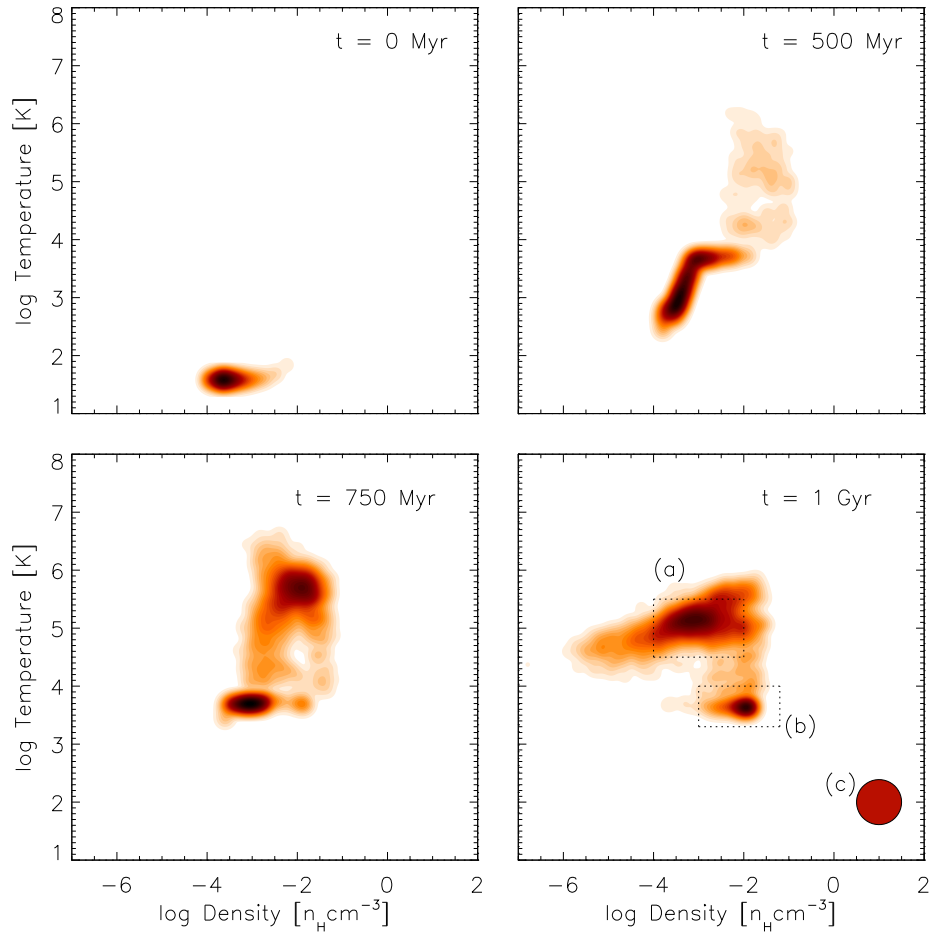
Figure 4.11: Density-Temperature relation for a rotating collapse simulation showing the creation of three distinct components. In the final time plot region *a* contains the supernova heated gas in the halo of the galaxy. *b* is gas contained in the disk of the galaxy, which reaches an equilibrium temperature of $\sim 10^4 K$ and *c* represents the approximate position of the molecular clouds, at an assumed temperature of $100 K$. Approximately 45% of the mass is in the hot phase, 40% in the disk and 15% in the cold molecular clouds.
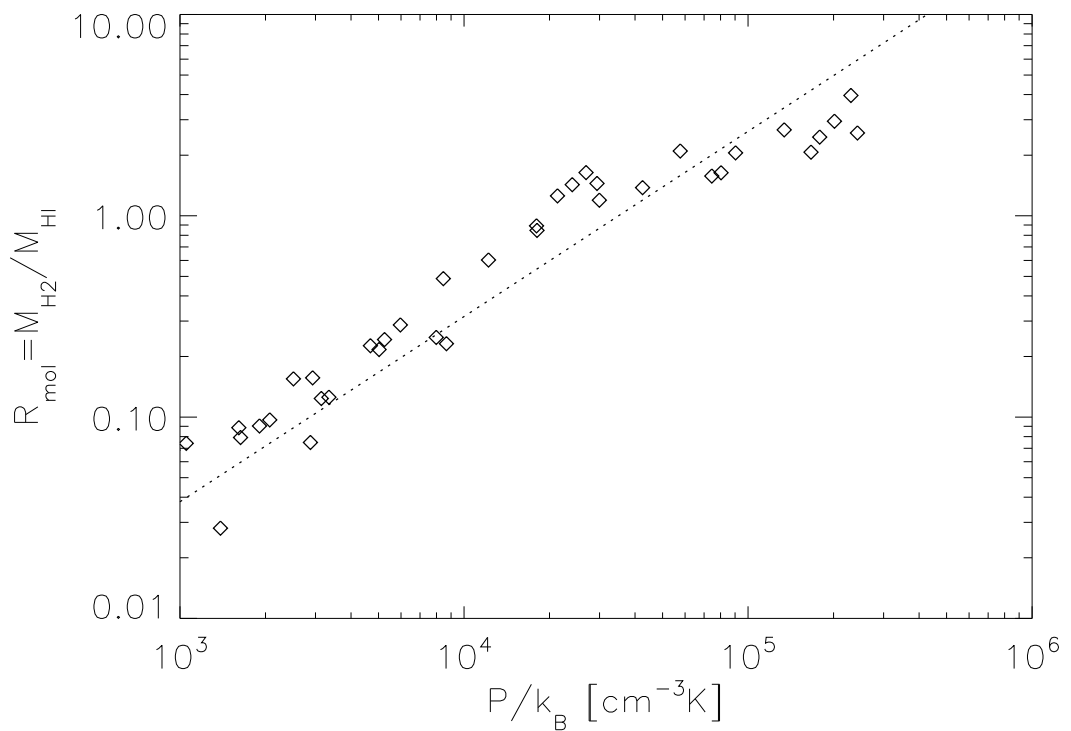
Figure 4.12: The relation between the pressure in the midplane of the galactic disk and the proportion of the gas in the molecular phase, R_{mol}. The dotted line represents the observational result (Eq (4.1)) due to Blitz & Rosolowsky (2006). The simulated galaxy is in good agreement with observation.

again behave in very similar ways. Fig (4.9) shows the radial density profile of stellar mass, demonstrating that our star formation prescription gives rise to an exponential disk and a bulge component well fitted by the standard $r^{1/4}$ law.

The rotating collapse simulations are especially interesting because they start far from equilibrium and so features that arise in the final particle distribution are purely an effect of the physics in the simulation and not just set up by hand in the initial conditions. Fig (4.10) shows how the molecular fraction (the ratio of the mass in molecular hydrogen to the mass in atomic hydrogen) varies as a function of distance from the centre. Observational data from M31 (Dame et al. (1993)) is included as a comparison.

The evolution of the thermal properties of the halo are shown in Fig (4.11). In its initial state all the gas in the halo is cold. As the halo collapses it becomes dense and is shock heated. The gas that ends up in the disk comes to an equilibrium between radiative cooling and the heating due to SNe at approximately $10^4 K$ and a halo of hot, SN heated gas at $\sim 10^6 K$ is gradually formed. The addition of the molecular gas ($T \sim$ 100K, $\rho \sim 100-1000\text{cm}^{-3}$) forms an ISM with four phases: shocked halo gas, SNe heated material, cold molecular clouds and warm disk gas. The first two components are hard to distinguish on the $\rho - T$ plot.

Blitz et al. (2006) have argued that the ratio of molecular to atomic gas in galaxies, R_{mol}, is determined by hydrostatic pressure and through observations of nearby galaxies found the following relation:

$$R_{\text{mol}} = \left[\frac{P_{\text{ext}}/k_B}{(3.5 \pm 0.6) \times 10^4} \right]^{0.92 \pm 0.07}, \tag{4.1}$$

where P_{ext} is an estimate of the mid-plane pressure. R_{mol} is the ratio of mass in the atomic and molecular phases. Fig (4.12) shows the data for the ROT_BASE simulation after 1 Gyr alongside the observed best fit line (Eq (4.1)). We use the SPH estimate of the pressure at $z = 0$. To calculate R_{mol} we use all matter within a vertical distance of 1kpc from the centre of mass of the disk and bin radially. The model of the ISM clearly reproduces the observed behaviour.

4.4 Away From the Base Model

The determination of some of the physical parameters used in our model is somewhat uncertain. In this section we investigate the effect of varying some of the physics included in the models. Large uncertainties are present in the determination of some of the
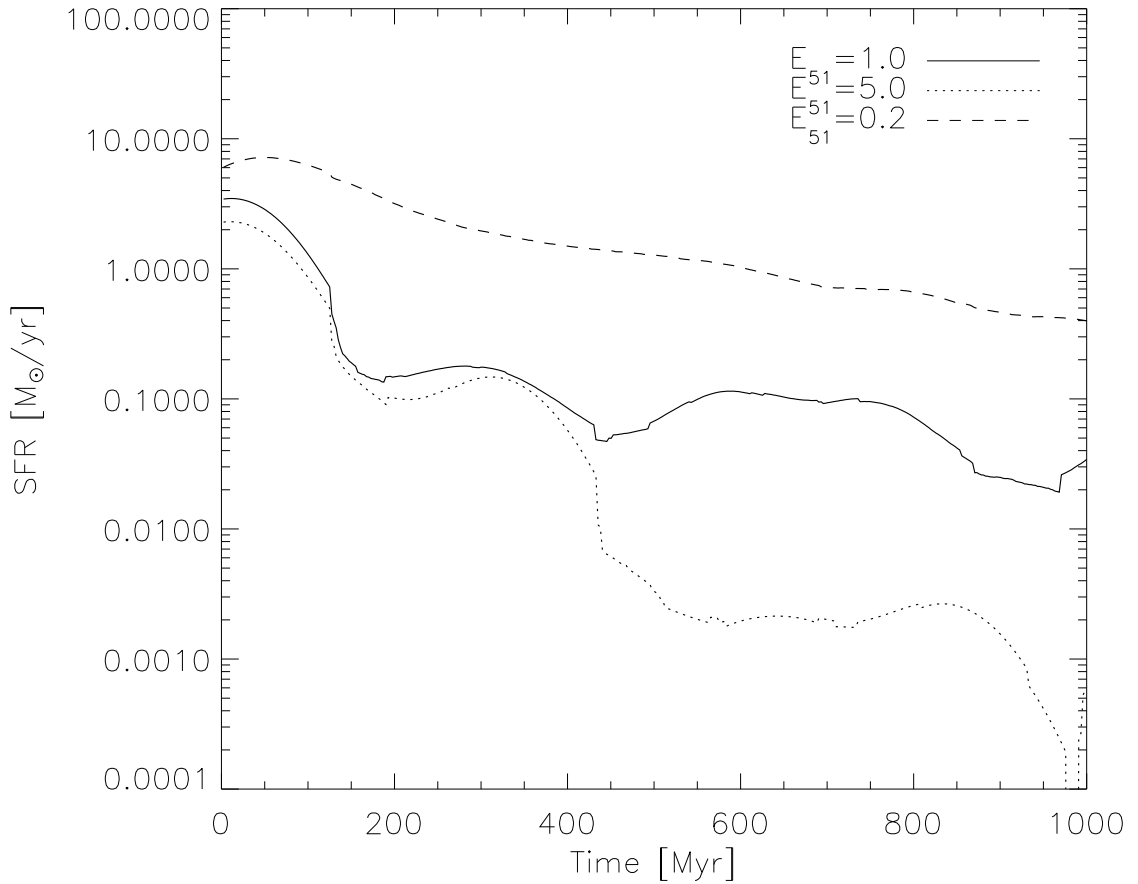
Figure 4.13: The star formation rates in the simulated disks for different values of E_{51}. Higher values of E_{51} effectively quench the star formation by heating and ejecting the ambient gas from the stellar disk.

parameters including E_{51}, the thermal conduction efficiency, and the physics we include in our treatment of supernova explosions. In addition our simulations do not contain a detailed treatment of metals. We demonstrate the effects of changing these parameters on the large scale properties of simulated galaxies.

4.4.1 Supernova Physics

In this section we investigate the effect of changing the parameters that govern the behaviour of supernova remnants. The value of E_{51} is poorly constrained by observation and may differ greatly from unity, for example due to radiative cooling of the supernova remnant. We investigate the effect of moving E_{51} away from unity and also look at changing the physics included in our analytic model for blast wave evolution, firstly
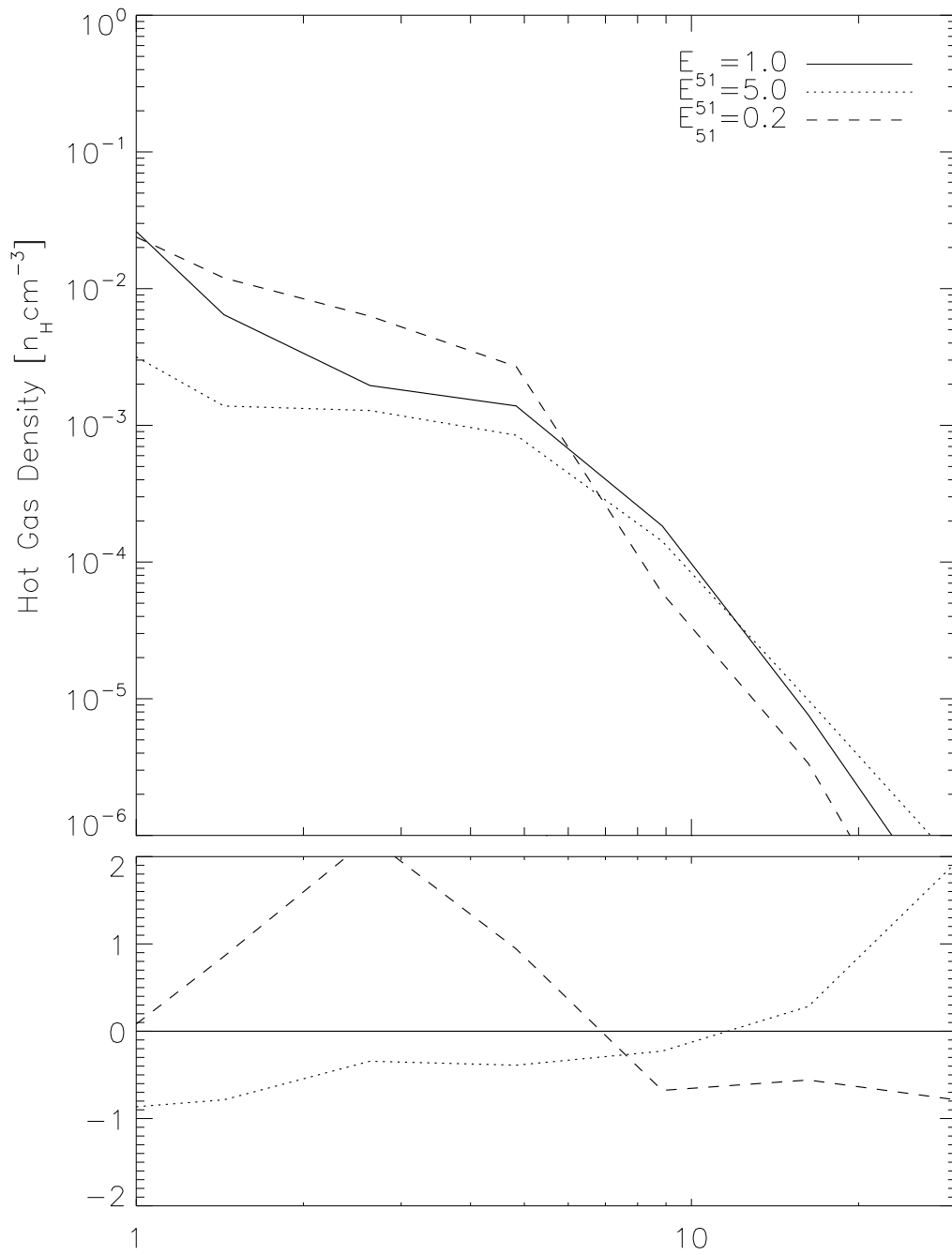
Figure 4.14: The ambient gas density profile in the simulated disks for three different values of E_{51}. The simulations with lower supernova efficiencies lead to more concentrated gas disks.

by extending the simple Sedov solution with the fitting formula due to Tang and Wang (2005) and secondly by investigating the effects of preventing radiative cooling in supernova remnants.

Altering the value of E_{51} has, as expected, two main effects. Firstly an increased supernova efficiency can eject gas from the galactic disk more efficiently and quenches star formation very quickly (fig 4.13). Secondly, the gas disk in simulations with higher supernova efficiency is found to be less concentrated (figure 4.14)

More accurate modelling of the evolution of supernova blast waves (by using the Tang and Wang (2005) fit to the blast wave evolution) does not significantly change the properties of the galaxy. Assuming that a typical supernova remnant expands for approximately ~ 0.3 Myr before being dispersed, that the mean ambient temperature of the ISM is 10^6 K and the mean density is 10^{-2} atoms per cm^3 then the difference in the blast wave radius between the pure Sedov solution (3.38) and the modified fitting formula due to Tang and Wang (2005) (Eq (3.39)) is never more than 20%. This is demonstrated in Fig 3.3, which shows a pure Sedov blast wave compared with the simulated result from an SPH simulation of a blast wave in a hot ($10^6 K$) medium.

The net result of having larger blastwaves is that the porosity of the ISM increases at a greater rate and the delay between a supernova explosion occuring and its thermal energy being injected into the ambient medium is decreased.

Finally we can switch off the radiative cooling in supernova remnants. The effects here are much more dramatic. In the dense galactic disk a supernova remnant can typically radiate away over 90% of its thermal energy before being disrupted. Switching off radiative cooling in supernova remnants, therefore, has a very severe effect in our galaxy simulations, and leads to the almost immediate suppression of star formation and much of the material in the galactic disk is ejected from the galaxy. This demonstrates that radiative losses from supernova remnants are of crucial importance in our models.

4.4.2 The Effects of Metals

Our simulation code does not contain a detailed description of mass feedback from supernovae, therefore we need to verify that the expected evolution in metallicity over the timescale of the simulation will not substantially affect the properties of the galactic disk.

Following Harfst et al. (2006) we use a simple analytic model to estimate the change in metallicity over the timescale of a typical simulation then run simulations with metallicites bracketing this range. By assuming that stars form at a constant rate of $1 M_\odot/\mathrm{yr}$,

that there is one type 2 supernova event per $125M_\odot$ of stars formed, and using metal yields due to Woosley and Weaver (1995) we estimate that over the 1Gyr timespan of one of the quiescent disk simulations the average metallicity of the galaxy should not change by more than $0.04Z_\odot$.

The base simulations have a metallicity of $1.0Z_\odot$, an additional two disk simulations were run with metallicities of $0.5Z_\odot$ and $1.5Z_\odot$, far outside the metallicity evolution range expected in our quiescent disks. The total amount of stars after 1Gyr in the high metallicity run is 5% higher than in the base run. The low metallicity run contains approximately 5% less stars than the base run. This trend arises because the radiative cooling rate of the ambient phase is related to the ambient gas metallicity. All the properties of the three simulated disks agree to within 10% with the properties of the base simulations.

However, as noted by Harfst et al. (2006) a detailed prescription for the yields from supernovae is necessary if we want to simulate the early evolution of a galaxy.

4.4.3 Thermal Conduction

One of the most poorly constrained parameters is the efficiency of evaporation of molecular clouds through thermal conduction. Magnetic fields and turbulence may affect the amount of thermal conduction by a large amount (MO77). We ran quiescent disk simulations with the efficiency of thermal conduction moved by a factor of five in each direction. The effects of varying thermal conduction on the cloud mass function can be seen in figure 4.15. More efficient thermal conduction leads to a lower density of molecular clouds in the galactic disk, as well as making the cloud mass function more shallow. The star formation rates are affected by a similar amount, in the simulations with a high thermal conduction rate the star formation rate is depressed by a large factor. As discussed in section 4.3 the base value for the thermal conduction efficiency reproduces many of the observed properties of the MW.
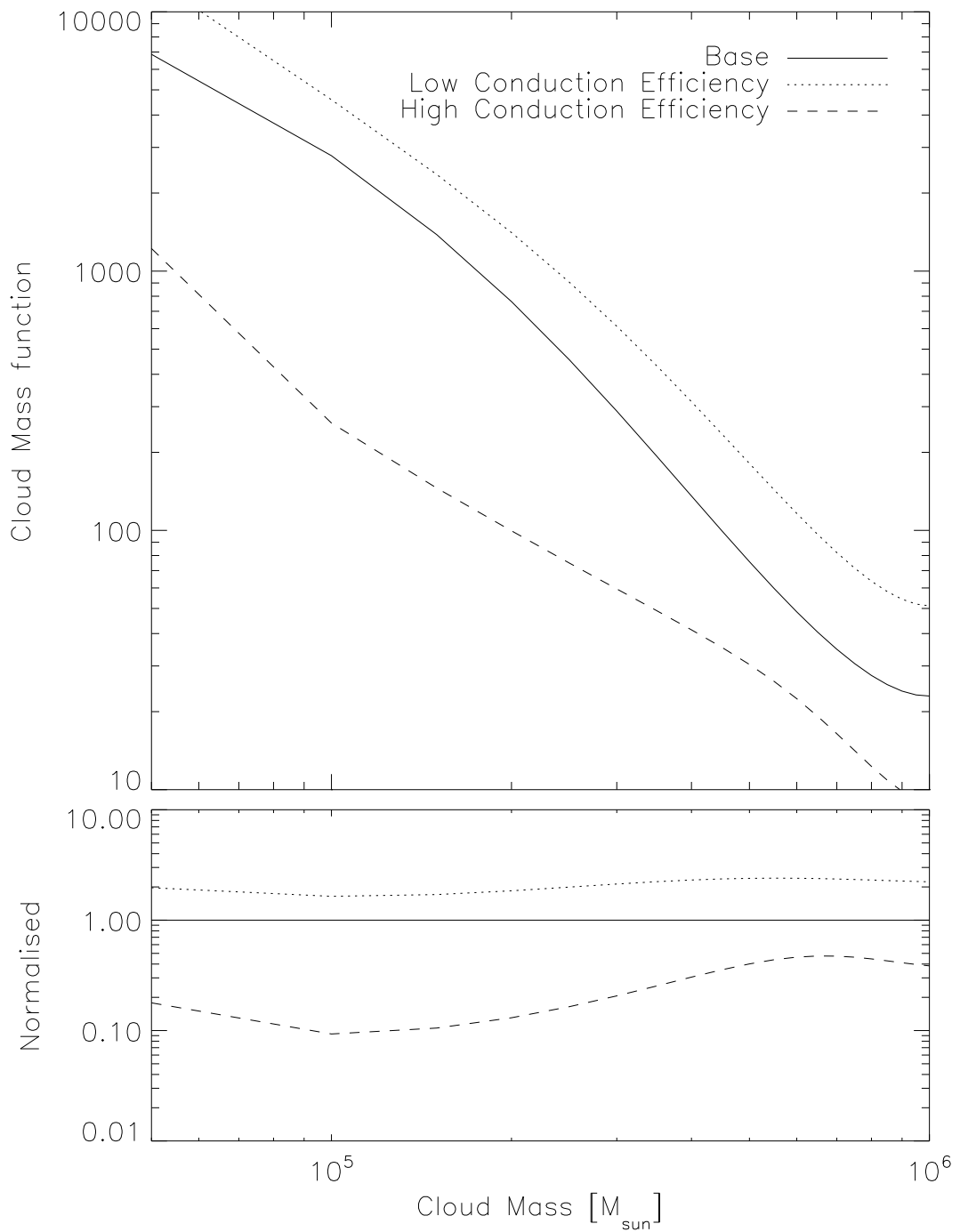
Figure 4.15: The effect of thermal conduction efficiency on the cloud mass spectrum of simulated galaxies. The upper plot shows the cloud mass functions for each galaxy, the lower plot shows the mass functions normalised to that of the base simulation. Higher thermal conduction efficiency leads to a lower density of molecular clouds and also a shallower molecular cloud mass function